Geophysical fingerprint of the 4-11 July 2024 eruptive activity at Stromboli volcano, Italy.

Luciano Zuccarello[1,2], Duccio Gheri[1], Silvio De Angelis[2,1], Riccardo Civico[3], Tullio Ricci[3], Piergiorgio Scarlato[3].

1Istituto Nazionale di Geofisica e Vulcanologia, Sezione di Pisa, via Cesare Battisti, 53, 56125, Pisa, Italy.
2School of Environmental Sciences, University of Liverpool, 4 Brownlow Street, L69 3GP, Liverpool, UK.
3Istituto Nazionale di Geofisica e Vulcanologia, Sezione Roma 1, via di Vigna Murata, 605, 00143, Roma, Italy.

Correspondence to: Luciano Zuccarello (luciano.zuccarello@ingv.it); Duccio Gheri (duccio.gheri@ingv.it)

Abstract. Paroxysmal eruptions, characterized by sudden and vigorous explosive activity, are frequent at open-vent volcanoes. Stromboli volcano, Italy, is well-known for its nearly continuous degassing activity and mild explosions from the summit craters, occasionally punctuated by short-lived paroxysms. Here, we analyse multi-parameter geophysical data recorded at Stromboli in early July 2024, during a period of activity that led to a paroxysmal eruption on 11 July. We use seismic, infrasound and ground deformation data, complemented by visual and Unoccupied Aircraft System observations, to identify key geophysical precursors to the explosive activity and to reconstruct the sequence of events. Elevated levels of volcanic tremor and Very Long Period seismicity accompanied moderate explosive activity, lava emission and small collapses from the North crater, leading to a major explosion on 4 July, 2024, at 12:16 (UTC). Collapse activity from the North crater area continued throughout 7 July, while effusive activity occurred from two closely-spaced vents located within Sciara del Fuoco, on the Northwest flank of the volcano. On 11 July, a rapid increase in ground deformation preceded, by approximately 10 minutes, a paroxysmal event at 12:08 (UTC); the explosion produced a 5 km-high eruptive column and pyroclastic density currents along Sciara del Fuoco. Our observations suggest that the early activity in July was linked to eruption of resident magma within the shallowest parts of the volcano plumbing. This was followed by lowering of the magma level within the conduit system as confirmed by the location of newly opened effusive vents. Rapid ground deformation before the paroxysmal explosion on 11 July is consistent with the expansion of a gas-rich magma rising from depth, similar to past energetic explosive events at Stromboli. Our findings offer valuable insights into Stromboli's eruptive dynamics and other open-conduit volcanoes, highlighting the importance of integrated geophysical observations for understanding eruption dynamics, forecasting, and associated risk mitigation.

1 Introduction

Stromboli is an open conduit stratovolcano located in the Tyrrhenian Sea, off the northern coast of Sicily; its activity is characterized by continuous degassing and frequent, small-to-moderate, explosions occurring every few minutes from the summit craters, the well-known Strombolian activity. However, activity at Stromboli can rapidly escalate into more energetic events, referred to as major explosions, which eject centimeter-to-meter-sized ballistic projectiles; at times, sustained explosive activity is accompanied by partial collapses of the crater rim (Gurioli et al., 2013; Di Traglia et al., 2024). Since 2019, major explosions at Stromboli have occurred with a frequency of about 4-5 events per year ejecting pyroclastic material to heights over a hundred meters, which can travel beyond the summit crater area and potentially affect tourist paths (Rosi et al., 2013; Gurioli et al., 2013). During periods of heightened activity, Stromboli may also experience paroxysms, that is highly energetic eruptions that generate eruptive columns exceeding 4 km in height, ballistics of up to 2 m in diameter and significant collapse activity from the summit crater areas (Fig. 1). Paroxysms can be accompanied by the emplacement of pyroclastic density currents (PDCs) along the Sciara del Fuoco (SdF, Fig. 1a), which can enter the sea and travel up to 2 km from the shoreline with demonstrated potential to trigger tsunamis (Rosi et al., 2006; Calvari et al., 2006; D'Auria et al., 2006; Ripepe and Lacanna, 2024). Although paroxysms are less frequent than major explosions, with an average occurrence of just one every four years since 2003, they are the most impactful hazard for the island of Stromboli (Rosi et al., 2013). For instance, the recent paroxysm occurred on 3 July, 2019, resulted in a fatality (Giudicepietro et al., 2020; Giordano and De Astis, 2020; Andronico et al., 2021).

Unrest and eruption at Stromboli generate a broad range of geophysical signals. Nucleation and coalescence of gas bubbles into gas slugs (Sparks, 2003; Burton et al., 2007; Caricchi et al., 2024), and their ascent within the conduit generates characteristic seismic and deformation signals (Marchetti et al., 2009); gas slug bursting at the top of the magma column produces infrasound waves (Colò et al., 2010). Real-time detection and monitoring of these signals are crucial for risk mitigation at Stromboli, in the recent past, major explosions and paroxysms have been anticipated by detectable changes in geophysical signals between tens of seconds and minutes before their occurrence (Giudicepietro et al., 2020; Ripepe et al., 2021a; Longo et al., 2024). Except for the 2019 eruptive activity, the most intense in recent years, Stromboli's paroxysms are typically preceded by periods of lava effusion, or a general increase in surface activity that lasts for several days (Ripepe et al., 2009; Valade et al., 2016). Several studies have suggested that effusive eruptions may act as a trigger for paroxysmal explosions through a mechanism of decompression of the volcano plumbing system, evidenced by a drop in magma levels within the conduit (Aiuppa et al., 2010; Calvari et al., 2011; Ripepe et al., 2017). The most significant effusive event in terms of its volume occurred between December 2002 and July 2003 (Ripepe et al., 2017), which caused landslides, triggered a partial collapse of the SdF and culminated in a paroxysm on 5 April, 2003; this was the first large-scale paroxysmal event recorded since 1985 (Calvari and Nunnari, 2023). However, it should also be noted that effusive eruptions are not necessarily followed by paroxysms. An example is the November 2014 effusive eruption, which did not lead to paroxysmal activity (Rizzo et al., 2015). At the other end of the spectrum lies the paroxysm of July 2019, for which no clear increase in activity prior to the main event was recorded. As highlighted by Laiolo et al. (2022), thermal and gas flow levels had slightly increased but remained below "alert" thresholds.

Multi-parameter data are crucial to understand unrest at Stromboli and to detect transitions between low-to-moderate activity and more explosive phases (Pistolesi et al., 2011; Andronico et al., 2021). A variety of models account for the occurrence and characteristics of seismic signal recorded at Stromboli and similar volcanoes (e.g., Chouet et al., 2008; Suckale et al., 2016;

Ripepe et al., 2021b). Petrological analyses suggest Stromboli's conduit is stratified, with two types of magma: highly porphyritic (HP) and low-porphyritic (LP) (Bertagnini et al., 2003; Francalanci et al., 2004, 2005). Eruptions are believed to result from gas slugs rising through the HP magma, which acts as a viscous plug controlling their ascent and explosion (Sparks, 2003; Burton et al., 2007; Aiuppa et al., 2010; Caricchi et al., 2024). A recent model by Caricchi et al. (2024) suggests that instability of gas-rich foam layers at the base of magma column could also trigger paroxysmal explosions.

In this study, we report on the most recent paroxysm at Stromboli, which occurred on 11 July, 2024, following a month of unrest at the summit craters, as reported by the Istituto Nazionale di Geofisica e Vulcanologia (INGV) (INGV-OE, 2024). We analyse the precursory geophysical activity leading up to the paroxysm based on seismic, infrasound and ground deformation data gathered by the INGV monitoring network, complemented by observations conducted with Unoccupied Aircraft Systems (UAS) during the study period. The UAS imagery provides a valuable tool to interpret geophysical data and understand the conditions leading up to the paroxysm on 11 July, offering a high-resolution reconstruction of the eruptive events and associated morphological changes at the volcano. Unless otherwise stated, all descriptions of surface activity in this manuscript are from direct field observations by the authors during the study period.

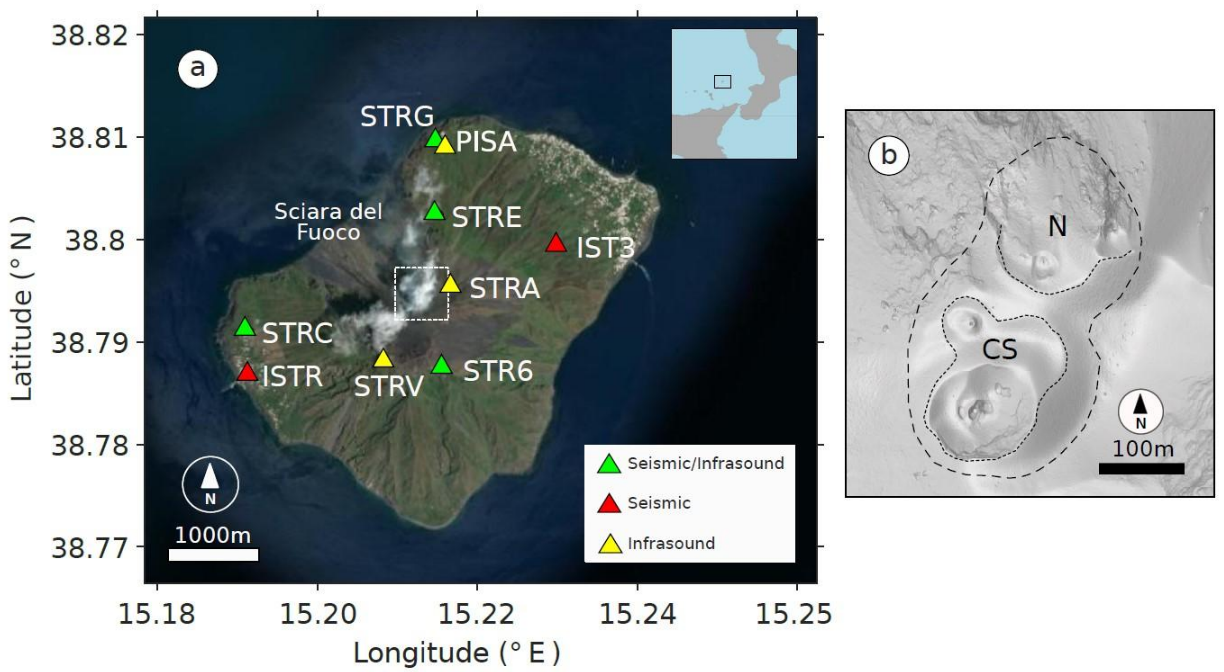

Figure 1: a) Map of monitoring network at Stromboli, showing the locations of seismo-acoustic, seismic, and infrasound sensors. The inset shows the location of Stromboli volcano in Italy (MATLAB Mapping Toolbox). b) Detail of the summit area of Stromboli, corresponding to the white dash-line square in a), showing the North (N) and Center-South (CS) summit crater areas.

2 Chronology of eruptive activity

The activity bulletins issued by INGV (see Data Availability), from 24 May until the early days of July, reported an increase in surface activity at Stromboli, particularly from the North (N) crater area (Fig. 1b), characterized by continuous and intense spattering, that is quasi-continuous emission of pyroclastic material through sequential, small-to-moderate, explosions ejecting ballistics at heights of ~10-20 m above the vent (Harris and Ripepe, 2007; Giudicedipietro et al., 2021) (Fig. 2a). The average frequency of explosions fluctuated between 13 (medium) and 16 (high) events/hour with spattering occasionally leading to lava flows along the SdF. On 23 and 28 June, lava flows began, following intense spattering from the N crater, converging into a canyon-like structure created by previous PDC activity in October 2022 (Di Traglia et al., 2024). Sulfur dioxide (SO_2) and carbon dioxide (CO_2) emissions remained at average levels, as did the carbon-to-sulfur (C/S) ratio (INGV-OE, 2024).

On 3 July, at 16:35 UTC, intense spattering was observed from a vent located within the N crater sector, leading to a sequence of partial collapses of the N crater rim, which also remobilized material that had been erupted in the preceding days. These collapses mostly consisted of cold material with a minor contribution of hot deposits. At 17:02 UTC, a lava flow began from the same vent, accompanied by spattering and moderate explosions (Fig. 2b). The activity continued throughout the night, with lava fronts moving down to an elevation of 550-600 m a.s.l..

On 4 July, at 12:11 UTC, a major explosion occurred from the N crater and, at 14:10 UTC, a new lava flow emerged at the base of the N crater area at ~700 m a.s.l., advancing towards Bastimento and Filo di Fuoco, located along the northeast boundary of SdF. After about one hour, a second lava flow started at an elevation of ~580 m a.s.l., which reached the sea. At 16:15 UTC, another vent opened at ~510 m a.s.l., producing a third lava flow accompanied by PDCs that rapidly descended the SdF into the sea (Fig. 2c). During the evening of 4 July, and throughout the following night, lava flow activity continued, accompanied by occasional collapses of pyroclastic materials.

Between 5-6 July, 83 landslide events were observed, while effusive activity fluctuated and lava emission moved further downslope originating from two new eruptive vents at ~485 m a.s.l. (Fig. 2d). The flow formed a delta at the shoreline and steam plumes were observed caused by magma-seawater interaction. Explosive activity from the summit craters halted at the beginning of the effusive phase.

On 11 July, at 12:08 UTC, a paroxysmal eruption occurred from the N crater area, producing an ash plume ~5 km high, which dispersed towards the southwest (Fig. 2e). Shortly after, a pyroclastic flow rapidly advanced along the SdF, which triggered a small-scale tsunami wave. The paroxysmal phase ended with a series of secondary and less intense PDCs.

In the following hours, effusive activity ceased, and no further explosions were observed, except for a minor event on 12 July, at 08:28 UTC (Fig. 2a), which was followed by a small collapse event in the N crater area.

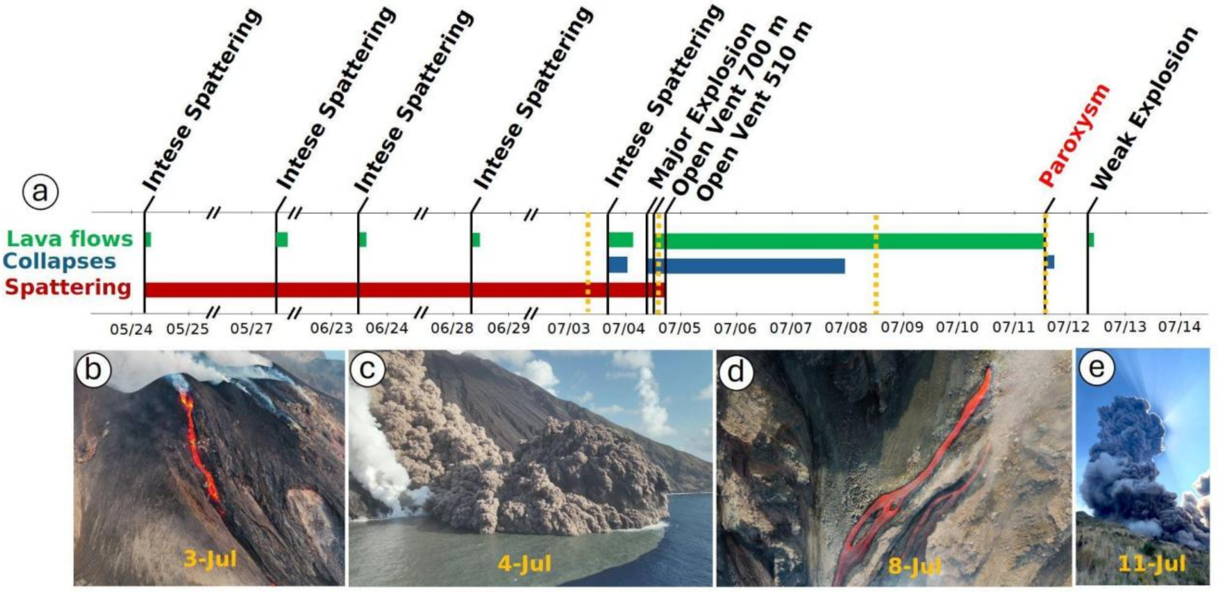

Figure 2: Timeline of the observed surface activity and key visual observations at Stromboli between late May and mid-July~~,~~ 2024. a) Timeline showing the chronology of activity, which marks periods of activity characterized by lava flows (green), collapses (blue) and spattering (red). Significant events are labelled, such as intense spattering, a major explosion on 4 July, opening of new vents, and the paroxysm on 11 July. b-e) Sequence of images gathered at the times indicated by the dashed yellow lines in a). From left to right: spattering activity on 3 July, a PDC event reaching into the sea on 4 July, continued lava flow on 8 July, and the paroxysmal explosion on 11 July (photo "e" courtesy of G. De Rosa - OGS).

3 Geophysical observations

In this study we use data recorded by the geophysical monitoring network deployed and maintained on Stromboli by INGV (Fig. 1a). The network includes two seismic broadband stations, equipped with Nanometrics Trillium (0.02–40 s) 3-component seismometers and Trident digital acquisition systems (IST3 and ISTR stations), as well as other four broadband station employing two GURALP CMG-3ESPC 120 s and two GURALP CMG-40T-60S seismometers (STR6 - STRE and STRC-STRG respectively). All the data recorded are digitized at 100 Hz.

The infrasound network includes five Chaparral microphones at the stations STRA, STRC, STRG, STRE and STR6, and a Geco srl sensor at STRV. Infrasound data are digitized at 100Hz (only STRA at 50 Hz) and recorded with 24-bit resolution using Guralp Affinity and Gaia2 digitizers (https://eida.ingv.it/; https://www.ov.ingv.it/index.php/ricercanew/stromboli). An additional infrasound station, called PISA (Fig. 1a), was deployed on 4 July at 13:35 UTC, 35 minutes before the onset of the effusive activity. Pisa was equipped with an IST-2018 broadband microphone, and the data were sampled at 100 Hz using DIGOS DATA-CUBE[3] 24-bit digitizer (e.g., Gheri et al., 2024).

3.1 Seismic characterization of eruptive events

Volcanic tremor is traditionally thought to reflect magma movement within the conduit (McNutt and Nishimura, 2008; Chouet et al., 1997; Ripepe and Gordeev, 1999); at Stromboli, volcanic tremor is routinely monitored by means of the Root Mean Square (RMS) of the continuous seismic signal (5-minut moving window) in the 1-3 Hz frequency band (Giudicepietro et al., 2023). Figure 3a shows RMS tremor amplitude values of the order of 10^{-6} ms^{-1} (recorded at the IST3 site), which correspond to tremor classified by INGV as high. A marked and short-lived increase in seismic RMS tremor amplitude was observed after the major explosion at 12:11 on 4 July (Fig. 3a). During this period, the signal reached unprecedented levels, peaking at 10^{-4} ms^{-1} at 17:00 UTC. Short-lived increases in RMS tremor amplitude values were still noted throughout 5~~,~~ July, although the RMS exhibited an overall decline to values of the order of 10^{-7} ms^{-1}, lower than those recorded at the beginning of July. In the following days (6-11 July), the RMS tremor amplitude was marked by a series of short-duration peaks during lava flow activity. This behaviour changed again on 11 July, when the onset of paroxysmal activity coincided with a new increase in RMS tremor amplitude (Fig. 3a). After the paroxysm, the RMS tremor amplitude decreased again with only sparse and brief intervals of increased amplitudes between 12-13 July (Fig. 3a). From late 13 July, onwards, the amplitude stabilized around 10^{-7} ms^{-1}, indicating that volcanic activity had reduced and returned to background levels. Additional details of the signals recorded on 4-11 July, are shown in the Supplementary Materials (Fig. 1Sa).

The spectrogram in Fig. 3b shows nearly continuous energy in the 1-3 Hz range, typically associated with tremor signals at Stromboli (Ripepe et al., 1996). Energy levels in this band change throughout the pre-, syn-, and post-explosive activity periods, peaking on 4 July (dark red in Fig. 3b) at 17:15 UTC, following the major explosion, which coincides with the RMS peak (see also Fig. 1Sce). A pulsating phase was observed from 6-11 July, with another peak during the paroxysm. Explosive activity between 4-11 July, exhibited a broader frequency range in the 0.5-15 Hz band. It is worth noting that the eruptive event on 4 July was preceded by a high-energy signal in the narrow frequency band 0.2-0.3 Hz (Fig. 3b). We also observe that this very low-frequency signal was not recorded before the paroxysm on 11 July. Finally, on 10 July at 05:09 UTC and on 11 July at 02:26 and 15:21 UTC, high-energy signals were observed around 0.05-0.08 Hz, exhibiting a dispersive spectrum typical of teleseismic events as reported by USGS (for further information, see: https://earthquake.usgs.gov/earthquakes/search/).

We have also analysed the occurrence of Very Long Period (VLP) earthquakes that have traditionally been associated with pressure disturbances and the dynamics of gas-rich magma within fluid-filled structures (Chouet et al., 1997; Chouet et al., 1999; Marchetti and Ripepe, 2005; Legrand and Perton, 2022), and one of the main tools used to monitor unrest at Stromboli. VLP events at Stromboli are thought to be generated by a pre-eruptive expansion due to rising pressure in the magma column, followed by a post-eruptive contraction as pressure decreases. Final oscillations in the VLP signal may be caused by fluctuations in the conduit or edifice. (Legrand and Perton, 2022). An increase in the frequency of occurrence of these signals is typically a precursor to periods of elevated eruptive activity (Ripepe et al 2009; Delle Donne et al., 2017). Figure 4a derived from information sourced from the INGV bulletins (INGV-OE, 2024), provides an overview of the rates of VLP seismicity at Stromboli between the end of May and mid-July 2024, after the 11 July paroxysm. From May until mid-June, VLP event rates remained stable, fluctuating around high values between 12 and 15 events/hour. A mean rate of ~13 events/hour is defined, at Stromboli, as “normal activity” (Ripepe et al., 2008) and it suggests that an efficient degassing mechanism of the magma column is established (Ripepe et al., 2021b). A significant peak is observed around mid-June, with the number of VLP events reaching 19 events/hour on June 16. This peak is followed by a slight decrease in event rates, although the number of events remained elevated compared to previous days. Figure 4b shows the characteristic compression-decompression cycle of VLP events at Stromboli; this waveform represents the normalized stack of all VLP events with maximum amplitude greater than 5×10^{-6} ms^{-1} at station STRE. Figure 4c, and more specifically 4d, shows a 1-day filtered (0.03-0.3Hz) seismic record illustrating the occurrence of VLP events as recorded at station STRE, the closest seismo-acoustic station to the eruptive area, located on the east flank of SdF at 495 m of elevation (see Fig. 1).

Before the major explosion on 4 July, we observed a clear drop in the occurrence of VLP events (Fig. 4a) from 10-15 to 7-10 events/hour. The rates of VLP events remained stable until the 11 July paroxysm, peaking again at 12 events/hour on that day. After the paroxysm, a further decrease in VLP rates was observed with hourly counts ranging from 6 to 10 events.

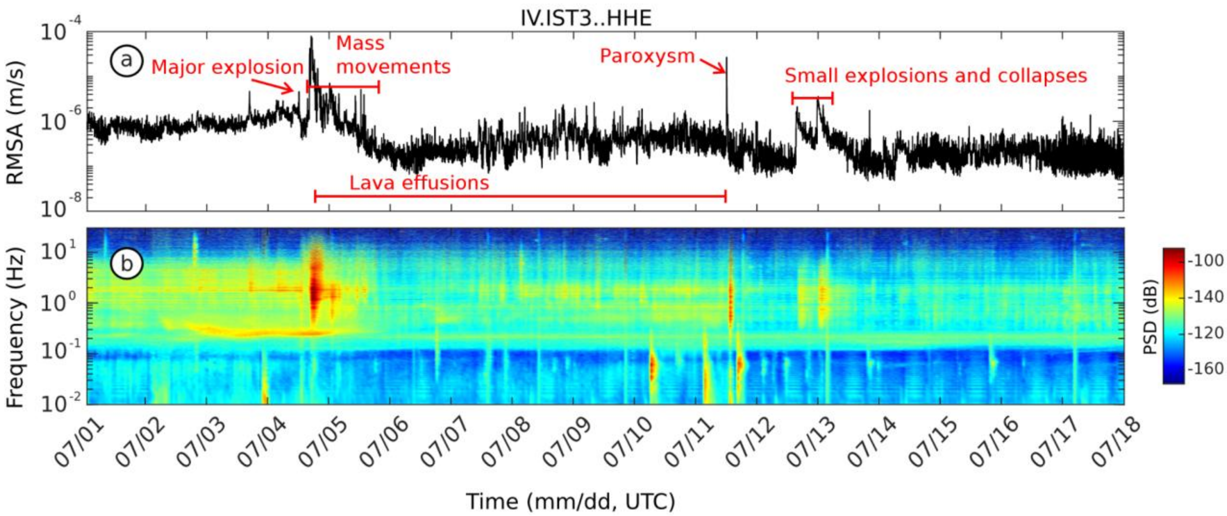

Figure 3: a) Seismic tremor or RMS tremor amplitude calculated every minute using a moving time window of 5 minutes, within the volcanic tremor frequency band of Stromboli (1-3 Hz), from 2 to 18 July. b) Spectrogram of the E-component from the IST3 seismic station for the same period.

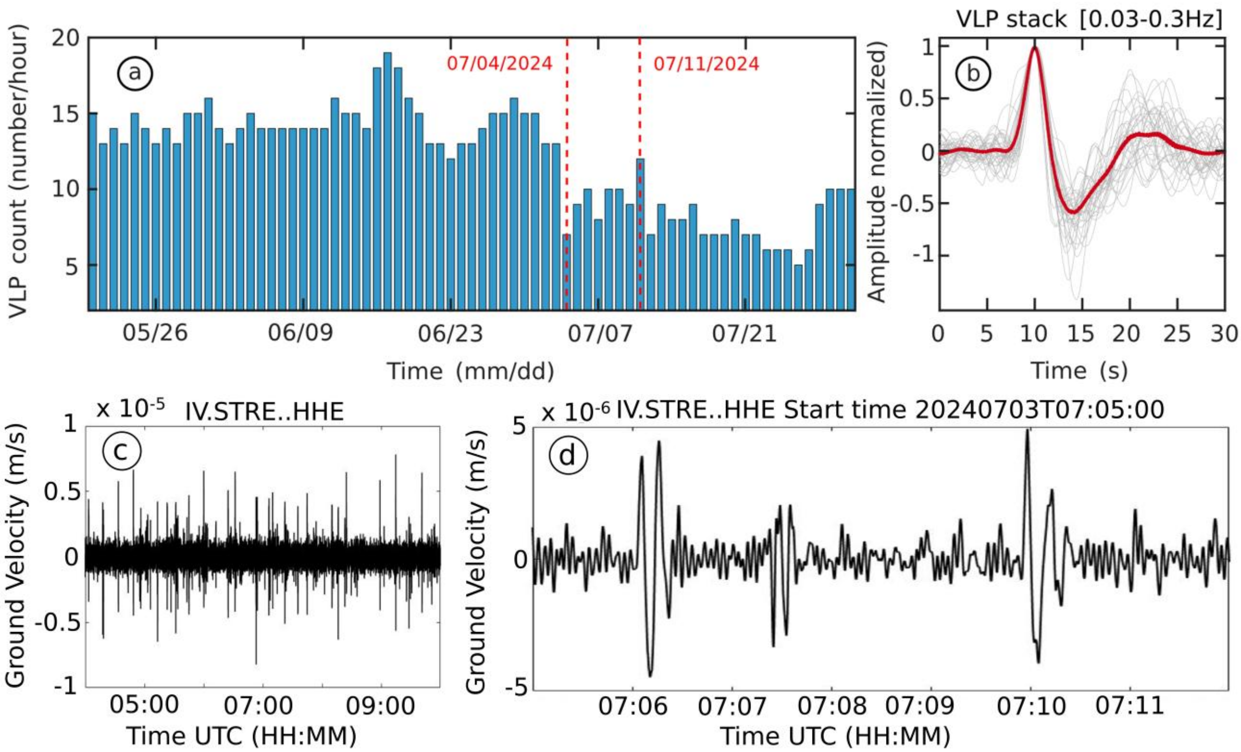

Figure 4: a) Hourly rates of VLP events from the INGV catalog. Vertical red dashed lines indicate the major explosion and paroxysm that occurred on 4 and 11 July, respectively. b) VLP waveform events (>5×10^{-6} ms^{-1}) recorded on 3 July, at station STRE normalized with respect to maximum amplitude (light grey). The red waveform represents the average of all high-amplitude waveforms. c) Continuous waveform recorded at station STRE (EW component) on 3 July 2024, filtered between 0.03-0.3 Hz. d) Extract from c) showing a sequence of VLP events recorded on 3 July over a 7-minute period by the STRE station on the same horizontal component

3.2 Infrasound location of the 11 July, 2024 paroxysm

We have also analysed infrasound data recorded by the INGV acoustic monitoring network and an additional microphone installed during the period of activity (Fig. 1). The infrasonic record before 4 July, shows a typical background of moderate strombolian activity occasionally interspersed with larger explosions (see Fig. 2Sa). The major explosion on 4 July, generated an infrasonic transient with a pressure of 5 Pa (Fig. 2Sb) at station STR6, ~750m from the CS crater area. Following this event, a marked decrease in acoustic energy was observed until the 11 July paroxysmal event, which produced infrasonic waves with a peak amplitude of 115 Pa at the STR6 site (at ~750 m from the source; see Fig.1a and Fig. 2Sc).

By analysing infrasound data, we located the source of the paroxysmal eruption on 11 July, 2024. We employed the RTM-FDTD (Reverse Time Migration - Finite Difference Time Domain) method of Fee et al. (2021), which implements waveform back-projection over a grid of candidate source locations. Travel-times between potential source locations and all stations in the network are calculated via FDTD modeling (Kim and Lees, 2014; Fee et al., 2017; Diaz-Moreno et al., 2019) to account for the effect of topography on the propagation of the acoustic wavefield. In the RTM-FDTD method, waveforms are backprojected and a detector function (e.g., network stack, network semblance) is evaluated for each candidate source, with the detector maximum corresponding to the most likely location. For FDTD calculations of travel-times we employed a UAS-derived Digital Elevation Model (DEM) of the SdF and the summit craters (Civico et al., 2024ab) areas conducted on the morning of 4 July with initial individual resolutions ranging between 20 and 50 cm/pixel. This DEM was merged with a reference elevation model (Civico et al., 2021) of the rest of the island, re-sampled, and parsed into a 5x5 m grid for the purpose of FDTD modeling. For FDTD modeling, the source time function was approximated by a Blackman-Harris function with a cutoff frequency of 5 Hz (high enough to include the dominant frequency of the explosion signals, between 0.2 and 2 Hz, while still allowing time-efficient computing) and the acoustic wavefield was propagated along the discretized topography using 15 grid points per wavelength (Wang, 1996). We used a constant sound velocity of 330 ms^{-1} (estimated from the signal move-out across the network) and a stratified atmosphere model based on density and temperature data obtained from the Reanalysis v5 (ERA5) dataset (see Data and Resources), produced by the European Centre for Medium-Range Weather Forecasts of the Copernicus Climate Change Service. We used data corresponding to the ERA5 grid node closest to Stromboli, at 12:00 on 11 July, 2024 (Coordinated Universal Time, UTC). The inferred source location for the paroxysmal explosion on 11 July, 2024, along with a record section of the infrasound waveforms used and the detector function, are shown in Fig. 5. The location identifies a source located approximately 50m below the rim of the N crater (Fig. 5a) at an elevation of ~685 m. The estimated origin time for the event is 12:08:52 UTC.

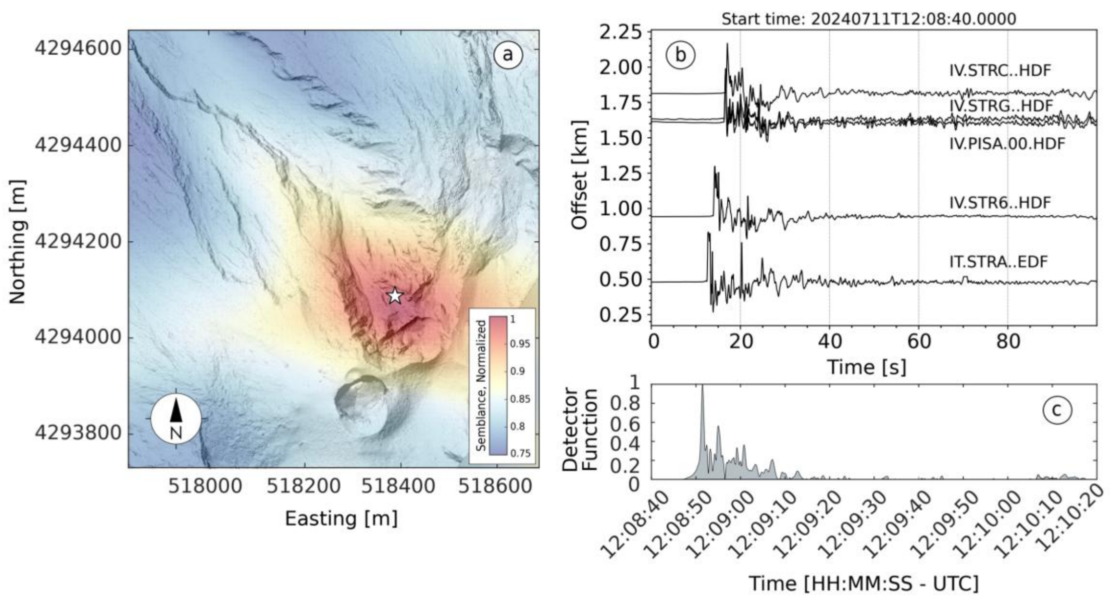

Figure 5: Infrasound location of the 11 July, 2024 paroxysmal event using the RTM-FDTD method (see manuscript for details; DEM of 14 July, 2024 from Civico et al. (2024a,b). a) Map-view of network semblance maximum around the Stromboli crater region. RTM-FDTD semblance location is indicated by a white star; b) record section of the filtered infrasound waveforms (bandpass filter 0.01-15Hz) used for locating the event. The offset corresponds to source-station distance; c) Normalized network detector function (i.e., maximum network semblance amplitude over time).

3.3 Tilt and eruptive events

Ground tilt at Stromboli has frequently been inferred to reflect processes like slug coalescence, slug ascent, and conduit emptying (Marchetti et al., 2009; Genco and Ripepe, 2010; Bonaccorso, 1998). Over the last decade, tilt has become central to real-time monitoring and eruption early warning at Stromboli. Ripepe et al. (2021a), for example, demonstrated the scale invariance of tilt at Stromboli, that is all explosions, regardless of their intensity, follow the same ground inflation-deflation pattern. A significant tilt was reported on 4 July (INGV-OE, 2024). The major explosion at 12:00 UTC was accompanied by a characteristic inflation-deflation pattern (Longo et al., 2024), followed by a pronounced deflation trend that began at 16:20 UTC and continued until 19:50 UTC (INGV-OE, 2024).

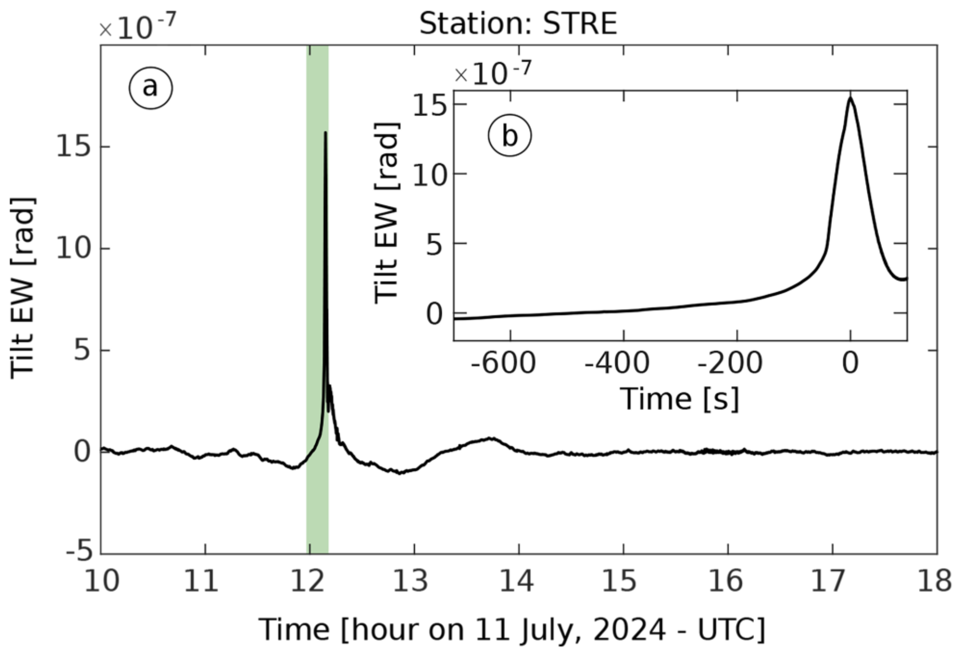

Figure 6: a) Radial tilt recorded by STRE broadband seismic station on 11 July, 2024; b) detail of tilt recorded before the 11 July paroxysm: the signal shows a marked amplitude increases starting ~10 minutes before the onset of the explosion.

For the paroxysm on 11 July, 2024 Fig. 6 shows the seismic-derived tilt, reconstructed from the EW horizontal component record at station STRE. The relationship between displacement and tilt sensitivity is a function of the long-period corner frequency of the seismometer used. By applying a magnification factor (e.g., Aoyama et al. (2008), Genco and Ripepe (2010) and De Angelis and Bodin (2012)), which is constant around the natural period of the seismometer, we were able to convert the seismometer's output from displacement to ground tilt. Slow inflation is observed, starting ~600 seconds before the explosion (Fig. 6b); the seismic-derived tilt sharply accelerates approximately 1 minute before reaching its peak of 1.5 µrad at the onset of the explosion, followed by rapid deflation. This pattern is consistent with previous observations of tilt at Stromboli before paroxysms and major explosions (e.g. Genco and Ripepe (2010) and Ripepe et al. (2021a)). We note that this tilt signal is derived from an individual seismic record, of an instrument that is not likely oriented in the direction radial to the source; for this reason, we will focus on the interpretation of the deformation trend and will not use the measured tilt amplitude for modelling purposes.

4 Discussion

In this manuscript we have presented geophysical data recorded between early and mid-July 2024 at Stromboli; the period of unrest included a major explosion on 4 July, significant collapse activity in the N summit crater area, emplacement of lava flows, and a paroxysmal event on 11 July. Surface activity at Stromboli intensified late in May with a marked increase in the occurrence of Strombolian explosions, the onset of effusive activity from SdF, and increasing volcanic tremor. Using multi-parameter observations, we reconstructed the chronology of the eruptive activity, which culminated in the paroxysmal explosion on 11 July, 2024.

4.1 Eruptive activity during the first week of July, 2024.

In the first week of July, we observed a steady increase in volcanic tremor reaching unprecedented amplitudes on 4 July, (see Fig. 3a and Fig. 1S). Volcanic tremor at Stromboli has typically been linked to the coalescence of gas bubbles from layers of smaller bubbles and their ascent along the shallower conduit (McNutt et al., 2008; Chouet et al., 1997; Ripepe et al., 1999), suggesting that variations in tremor intensity are controlled by changes in gas flow within the conduit.

It has been frequently speculated that an increase in volcanic tremor reflects an increase in the volume of gas within the magma (Ripepe et al., 1996), which in turn is linked to a higher occurrence of explosions at the top of the magma column. Field observations of increasing spattering in early July (Fig. 1) support a model of increased surface activity linked to the ascent of gas-rich magma within the shallow conduit. The spattering activity observed at the start of our study period represents an intensified form of puffing. Spattering results from the quasi-continuous bursting of small gas pockets within a bubbly flow regime, which generates pyroclasts (Rosi et al., 2013). This activity typically marks the initial stages of unrest and eruption at Stromboli, where gas-rich magma is actively degassed through continuous explosive bursts (Del Bello et al., 2012). The high rates of VLP events observed during the same period further support the hypothesis of gas-rich magma migration within the shallow plumbing system. These events are traditionally linked to the rapid expansion of gas bubbles rising through the liquid melt in the shallow conduit (Chouet et al., 2003; James et al., 2006); more recently Ripepe et al. (2021) suggested that VLP waveforms at Stromboli are generated at the top of the magma column, mainly after the onset of Strombolian explosions; they showed that the occurrence of VLP event can be linked to explosive magma decompression in the uppermost ~ 250 m of the conduit. The recorded VLP events showed similar waveforms (Fig. 4b) suggesting a stable source mechanism and location; locations in the shallow parts of the conduit can be linked to magma accumulation at a shallow depth, close to the surface. While the number of VLP events did not show any significant variation before the major explosion on 4 July, volcanic tremor increased slowly but steadily (Fig. 3a). Coinciding with strong ground deflation after the major explosion (INGV-OE, 2024), volcanic tremor reached an unprecedented peak amplitude of ~8 x 10^{-5} m s^{-1} at ~17:00 UTC associated with the opening of a new effusive vent at ~ 510 m elevation within SdF (Fig. 2a) and the occurrence of numerous mass wasting events linked to collapse activity within the lower N crater area and upper section of SdF. We suggest that these signals reflect the emptying of the shallowest parts of the conduit system and the overall lowering of the magma level within the shallow volcano plumbing reflected in the opening of new effusive vents at progressively lower elevations. The transition between explosive and effusive regimes was also marked by a clear decrease in the occurrence of VLP events (Fig. 4), and a migration of their source deeper within the conduit (as reported by the automatic seismic monitoring of INGV Osservatorio Vesuviano: http://eolo.ov.ingv.it/eolo/) and as already observed during past unrest by Ripepe et al. (2015). This contrasts with the flank eruptions of 2007 and 2014 (Ripepe et al., 2009; 2015) when VLP rates remained high during effusion; in July, 2024 it appears that effusion reduced the overall explosivity through progressive degassing of the shallow magma rather than recalling fresh, gas-rich, magma from depth. The new effusive regime, indeed, was characterized by a substantial lack of Strombolian explosive activity at the surface between 4-11 July, as observed in the field by our research team. The quasi-continuous collapse activity, observed from 13:00 UTC on 4 July, appeared to be linked to instabilities in the crater area around newly created vents; this instability persisted in the following days, with the number of events peaking on 5 July (83 recorded occurrences recorded in a single day (INGV-OE, 2024)). The collapse activity recorded along the N crater rim, adjacent to the SdF, resulted in significant changes to the morphology of this sector of the volcanic edifice (Fig. 7).

4.2 Eruptive activity during the second week of July, 2024.

The effusive regime, that began on 4 July, ended with the occurrence of the paroxysmal explosion on 11 July. The explosion generated an infrasonic pressure of 115 Pa at station STR6 with an associated VLP peak amplitude of 5.8 x 10^{-5} ms^{-1} (see Fig. 3S). The associated ash plume reached a height of 5 km above the vent, and pyroclastic flows moved down the SdF. After that, volcanic activity reduced its intensity, accompanied by low levels of tremor and VLP events; tremor increased again on 12~~,~~ July, associated with emplacement of a small lava flow.

The eruptive crisis of July 2024, culminating into the 11 July paroxysm, is consistent with previous eruptions at Stromboli, such as those in April 2003, March 2007, and July-August 2019. The observations that we have presented in this manuscript can be used to inform a conceptual model of the entire sequence of processes responsible for the observed surface and eruptive activity, within the framework of previous studies (e.g., James et al., 2006; Chouet et al., 2008; Del Bello et al., 2012; Suckale et al., 2015; McKee et al., 2022).

At the more explosive end of the spectrum of Strombolian activity major explosions and paroxysms are often explained invoking the "slug model" (James et al., 2006; Chouet et al., 2008; Del Bello et al., 2012). In this model, gas bubbles (slugs) form deeper in the magma column and gradually coalesce as they rise through the conduit due to an increase of the magma viscosity. As gas slugs ascend, they expand due to the decreasing confining pressure and eventually reach the surface. When they burst at the top of the magma column, they release gas explosively, fragmenting the magma and producing pyroclasts and feeding ash plumes of varying sizes. After the major explosion on 4 July, an effusive regime was established, characterized by lava flows, during which more degassed magma was erupted. Following the initial explosive activity driven by gas slugs, we infer that the transition to the effusive regime was controlled by depressurization of the shallow plumbing system similar to the model of Ripepe et al. (2017). The depressurization of the system caused by the initial explosive activity allowed magma to flow and reach the surface forming lava flows, without further explosive activity. As the shallow volcanic conduit progressively emptied it led to structural instability, causing collapses and landslides along the SdF.

According to Ripepe et al. (2017), the emptying of the conduit creates a “vacuum” effect that draws more gas-rich magma from deeper within the system. As volatile-rich magma rises and experiences lower pressures, activity can be triggered, sometimes resulting in a paroxysmal event. The dynamics of the 11 July paroxysmal explosion shared similarities across seismic, acoustic, and deformation parameters with past events (Genco and Ripepe, 2010; Ripepe et al., 2021a). This consistency further validates the established models of activity and Stromboli, where the largest explosions and energetic events, such as paroxysms, are driven by the same source mechanism. The scale-invariant conduit dynamics of ground deformation demonstrate that inflation amplitude and duration scale directly with the magnitude of the explosion (Ripepe et al., 2021a). Ground deformation observed on 11 July (Fig. 6) follows the same exponential inflation pattern as seen in previous paroxysms (Ripepe et al., 2021a). This behaviour is typically explained by bubble dynamics, where the pressure on the conduit walls increases due to the rapid volumetric expansion of gas in highly vesciculated magma. As gas rises and expands, it pushes the magma column toward the surface, often leading to precursory lava emissions from the vent. Ground deformation is likely caused by a combination of increasing magma static pressure and the pressurization of degassed magma at the top of the column, driven by the exponential expansion of the gas phase. When the pressure applied by the gas-rich magma exceeds the tensile strength of the viscous magma plug, fragmentation occurs, resulting in the explosive release of gas and pyroclastic material (e.g. paroxysm). Another possible mechanism, proposed by Suckale et al. (2016) and McKee et al. (2022) suggests that the explosion is triggered by the rapid expansion and release of gas when a partial rupture occurs in the plug at the top of the magma column.

4.3 Morphological changes of the crater area caused by the explosive activity.

During the study period, we also collected UAS data and compiled very high-resolution repeat DEMs (0.2-0.5 m/pixel), which allowed quantifying topographical changes via DEM differencing. The difference between DEMs on 4-July (morning; Civico et al., 2025) and 14 July (Civico et al., 2024ab) is shown in Fig. 7c. The data processing methodology follows procedures described in Civico et al. (2022, 2024a). The most notable morphological variations were observed in the afternoon of 4 July, while the paroxysm on 11 July did not lead to significant changes.

The summit craters experienced loss of material due to the opening of two eruptive vents at approximately 700 and 500 m a.s.l.. While the CS crater sector showed a roughly circular crater floor deepening of about 84 m, the N sector was affected by the complete dismantling of its northern rim and external slope, marking the deepest morphological change observed at the summit craters in the last decade, with a maximum difference in altitude of 109 m. The total volume loss recorded in the summit craters sector was estimated at 3.3 Mm^3 (Civico et al., 2024a).

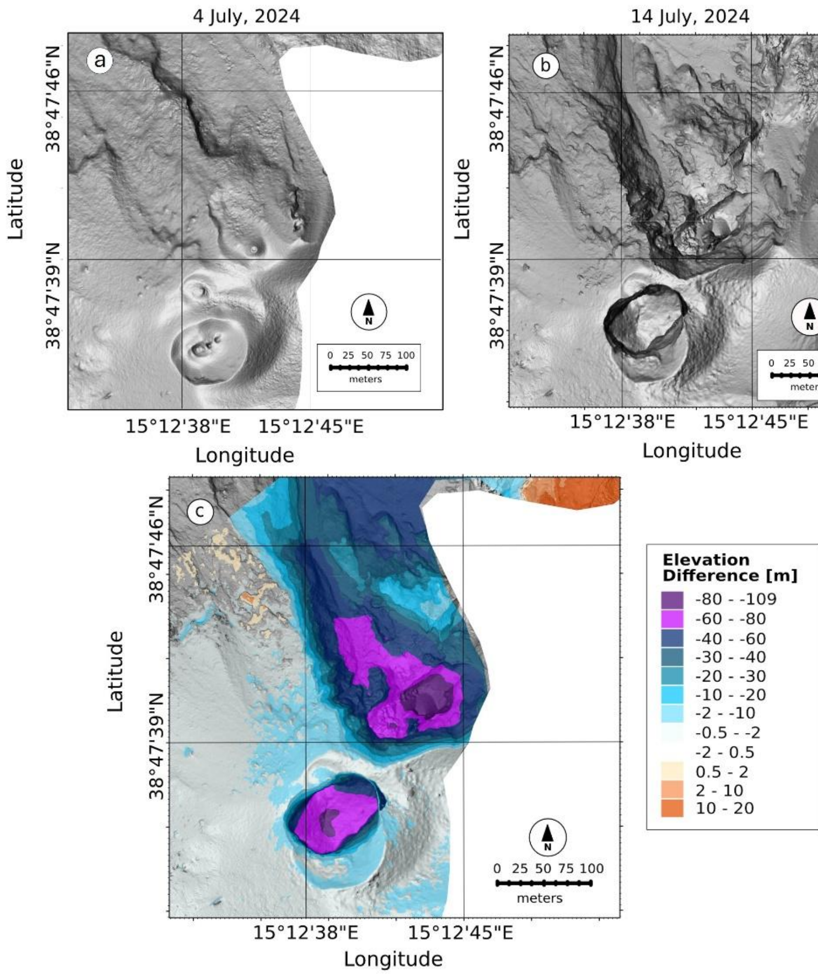

Figure 7: Multidirectional hillshade plots of Stromboli's crater area: a) 4 July, 2024 (Civico et al., 2025), b) 14 July, 2024 (Civico et al., 2024a,b), c) map of elevation difference (Dem of Differences) highlighting morphological changes between 4 and 14 July, 2024. Purple areas indicate material loss, whereas orange areas indicate material gain.

Unlike the summit craters, the subaerial portion of the SdF slope was affected by both accumulation and erosion processes. Here, the main loss of material (2.74 Mm^3; Civico et al., 2024a) was localized along the canyon formed in October 2022 (Di Traglia et al., 2024), which widened and deepened during the July 2024 eruption. On the other hand, accumulation processes instead were mainly due to PDC and lava flow deposits within the northeastern sector of the edifice. The maximum accumulation of lava occurred at the new lava delta (maximum difference in altitude of 45 m), located in the center of the SdF shoreline (Civico et al., 2024a).

5 Conclusion

The eruptive activity at Stromboli starting from 4~~,~~ July, and culminating with a paroxysm on 11~~,~~ July, 2024, provides a comprehensive case study of explosive volcanism at open-conduit volcanoes and offers valuable insights into its causative processes and mechanism.

The July 2024 paroxysm was preceded by a prolonged phase of heightened activity, characterized by increased volcanic tremor and VLP events. The elevated levels of seismicity, combined with observed crater rim collapses and lava flows, suggest a progressive destabilization of the volcanic edifice. In particular, the major explosion on 4 July and the subsequent paroxysm on 11 July highlight the role of magma gas dynamics, where increased gas volumes and pressure led to significant eruptive events.

Analysis of the seismic records reveals that the volcanic tremor intensity is linked to gas-rich magma movement, reaching in this eruptive sequence unprecedented values at Stromboli. However, the variability in VLP events indicates that, while useful for monitoring overall volcanic unrest, these signals alone may not serve as reliable precursors for major explosive events. Instead, the combined analysis of different geophysical parameters, including ground deformation, proved crucial for early warning and forecasting as previously suggested by Ripepe et al. (2021a).

Ground deformation patterns, specifically the inflation-deflation cycle observed before explosions, align with previous studies, confirming that such patterns reflect the occurrence of imminent explosions regardless of their magnitude. The exponential inflation observed before the paroxysm, caused by gas expansion and the rise of slugs within the magma column, is the same as in other paroxysmal events at Stromboli.

Through UAS data, Civico et al. (2024a) were able to estimate a total volume loss of about 6.0 Mm^3 involved after the gravitational mass collapses occurred on 4 and 11 July. The partial collapses generated a reshaping of the summit craters area as well as a deepening 2022 canyon along SdF, thus increasing flank instability.

In conclusion, our results demonstrate how geophysical, visual observation and UAS-derived topographic data offer new, valuable, insights for tracking and characterizing the processes that control the onset of volcanic explosive activity at Stromboli and other similar volcanoes. We suggest that multi-parameter volcano monitoring will lead to further significant advances in volcanic hazard mitigation.

Data availability

Seismic waveform data used in this study are from the INGV seismic network. All data are publicly available from EIDA Italia (https://eida.ingv.it/). Infrasound data are available upon request from the INGV- Osservatorio Vesuviano or direct enquiry to the authors of this manuscript. The infrasound data from PISA station are available at https://doi.org/10.5281/zenodo.14245572.

Author contribution

L.Z., S.D.A. and P.S. wrote the research proposals that funded the installation and maintenance of the infrasound array and UAS, designed the field experiment, and financially supported this publication. L.Z. and S.D.A. tested the infrasonic equipment, organized fieldwork and participated in the original design of the experiment. L.Z., S.D.A., R.C., T.R. contributed to assembling the final multiparametric dataset and tested its quality and retrieval. L.Z., R.C. and T.R. installed and maintained the equipment during the field acquisition. L.Z, S.D.A. and D.G. performed analyses of infrasound data, seismic and tilt data, and prepared all figures. R.C. and T.R. acquired and analysed the UAS images. L.Z. D.G. and S.D.A. jointly wrote the initial draft of the manuscript and all authors contributed to review and edit the final version.

Competing interests

The authors declare that they have no conflict of interest.

Acknowledgements

INGV Project ‘Pianeta Dinamico (Dynamic Planet) - Working Earth’: Geosciences For The Understanding The Dynamics Of The Earth And The Consequent Natural Risks - “Dynamo - DYNAmics of eruptive phenoMena at basaltic vOlcanoes” (https://progetti.ingv.it/it/pian-din/dynamo#project-info).

INGV Departmental Strategic Project “UNO - UNderstanding the Ordinary to forecast the extraordinary: An integrated approach for studying and interpreting the explosive activity at Stromboli volcano” (https://progetti.ingv.it/it/uno-stromboli).

L.Z., D.G., S.D.A., R.C., T. R: and P.G. are supported by the grant "Progetto INGV Pianeta Dinamico” - Sub-project VT_DYNAMO 2023 - code CUP D53J19000170001 - funded by Italian Ministry MIUR (“Fondo Finalizzato al rilancio degli investimenti delle amministrazioni centrali dello Stato e allo sviluppo del Paese”, legge 145/2018).

We are indebted to all the INGV colleagues who have contributed to the monitoring efforts on Stromboli during July 2024 and the ones involved in the surveillance and network maintenance activities, to Maria Zagari (Italian Civil Aviation Authority - ENAC) for her help in issuing new NOTAMs during the emergency, and to Giuseppe De Rosa, Istituto Nazionale di Oceanografia e di Geofisica Sperimentale (OGS) for providing the photo of the 11 July paroxysm in Fig. 1.

The contents of this article represent the authors’ ideas and do not necessarily correspond to the official opinion and policies of the Dipartimento della Protezione Civile - Presidenza del Consiglio dei Ministri. We are grateful to the colleagues of INGV -Osservatorio Vesuviano- for their support in the data management.

Financial support

This work was supported by the grant "Progetto INGV Pianeta Dinamico” -Sub-project VT_DYNAMO 2023- code CUP D53J19000170001 - funded by Italian Ministry MIUR (“Fondo Finalizzato al rilancio degli investimenti delle amministrazioni centrali dello Stato e allo sviluppo del Paese", legge 145/2018) and by NGV Departmental Strategic Project "UNO - UNderstanding the Ordinary to forecast the extraordinary: An integrated approach for studying and interpreting the explosive activity at Stromboli volcano".

References

Aiuppa, A., Burton, M., Caltabiano, T., Giudice, G., Guerrieri, S., Liuzzo, M., and Salerno, G.: Unusually large magmatic CO2 gas emissions prior to a basaltic paroxysm, Geophys. Res. Lett., 37, https://doi.org/10.1029/2010GL044997, 2010.

Andronico, D., Del Bello, E., D'Oriano, C., Landi, P., Pardini, F., Scarlato, P., and Valentini, F.: Uncovering the eruptive patterns of the 2019 double paroxysm eruption crisis of Stromboli volcano, Nat. Commun., 12, https://doi.org/10.1038/s41467-021-23349-4, 2021.

Bertagnini, A., Métrich, N., Landi, P., and Rosi, M.: Stromboli volcano (Aeolian Archipelago, Italy): An open window on the deep-feeding system of a steady state basaltic volcano, J. Geophys. Res. Solid Earth, 108, https://doi.org/10.1029/2002JB002146, 2003.

Bonaccorso, A.: Evidence of a dyke-sheet intrusion at Stromboli Volcano inferred through continuous tilt, Geophys. Res. Lett., 25, https://doi.org/10.1029/98GL00766, 1998.

Burton, M., Allard, P., Murè, F., and La Spina, A.: Magmatic gas composition reveals the source depth of slug-driven Strombolian explosive activity, Science, 317, https://doi.org/10.1126/science.1141900, 2007.

Calvari, S., Spampinato, L., and Lodato, L.: The 5 April 2003 vulcanian paroxysmal explosion at Stromboli volcano (Italy) from field observations and thermal data, J. Volcanol. Geotherm. Res., 149, https://doi.org/10.1016/j.jvolgeores.2005.09.008, 2006.

Calvari, S., Spampinato, L., Bonaccorso, A., Oppenheimer, C., Rivalta, E., and Boschi, E.: Lava effusion—A slow fuse for paroxysms at Stromboli volcano? Earth Planet. Sci. Lett., https://doi.org/10.1016/j.epsl.2011.03.005, 2011.

Calvari, S., and Nunnari, G.: Statistical insights on the eruptive activity at Stromboli volcano (Italy) recorded from 1879 to 2023, Remote Sensing, 15, https://doi.org/10.3390/rs15174298, 2023.

Caricchi, L., Montagna, C. P., Aiuppa, A., Lages, J., Tamburello, G., and Papale, P.: CO2 flushing triggers paroxysmal eruptions at open conduit basaltic volcanoes, J. Geophys. Res.: Solid Earth, 129, https://doi.org/10.1029/2023JB02561, 2024.

Chouet, B., Saccorotti, G., Martini, M., Dawson, P., De Luca, G., Milana, G., and Scarpa, R.: Source and path effects in the wave fields of tremor and explosions at Stromboli Volcano, Italy, J. Geophys. Res.: Solid Earth, 102, https://doi.org/10.1029/96JB03395, 1997.

Chouet, B., Dawson, P., Ohminato, T., Martini, M., Saccorotti, G., Giudicepietro, F., De Luca, G., Milana, G., and Scarpa, R.: Source mechanisms of explosions at Stromboli Volcano, Italy, determined from moment-tensor inversions of very-long-period data, J. Geophys. Res.: Solid Earth, 108, https://doi.org/10.1029/2002JB001919, 2003.

Chouet, B., Dawson, P., and Martini, M.: Shallow-conduit dynamics at Stromboli Volcano, Italy, imaged from waveform inversions, Geol. Soc. London, Special Publications, 307, https://doi.org/10.1144/SP307.5, 2008.

Colò, L., Ripepe, M., Baker, D. R., and Polacci, M.: Magma vesiculation and infrasonic activity at Stromboli open conduit volcano, Earth Planet. Sci. Lett., 292, https://doi.org/10.1016/j.epsl.2010.01.041, 2010.

Civico, R., Ricci, T., Scarlato, P., Andronico, D., Cantarero, M., Carr, B. B., De Beni, E., Del Bello, E., Johnson, J. B., Kueppers, U., Pizzimenti, L., Schmid, M., Strehlow, K., and Taddeucci, J.: Unoccupied Aircraft Systems (UASs) Reveal the Morphological Changes at Stromboli Volcano (Italy) before, between, and after the 3 July and 28 August 2019 Paroxysmal Eruptions, Remote Sensing, 13, https://doi.org/10.3390/rs13010141, 2021.

Civico, R., Ricci, T., Cecili, A., and Scarlato, P.: High-resolution topography reveals morphological changes of Stromboli volcano following the July 2024 eruption, Sci. Data, 11, 1219, https://doi.org/10.1038/s41597-024-04098-y, 2024a.

Civico, R., Ricci, T., Scarlato, P.: High-Resolution SfM Topography of Stromboli volcano (Italy), 14 July 2024. OpenTopography. https://doi.org/10.5069/G9S75DJH, 2024b. Accessed: 2025-02-05

Civico, R., Ricci, T. Scarlato, P.: SfM Topography of Stromboli volcano (Italy), 04 July 2024 – crater terrace. OpenTopography. https://doi.org/10.5069/G9T151WP, 2025. Accessed: 2025-02-05

D’Auria, L., Giudicepietro, F., Martini, M., and Peluso, R.: Seismological insight into the kinematics of the 5 April 2003 vulcanian explosion at Stromboli volcano (southern Italy), Geophys. Res. Lett., 33, https://doi.org/10.1029/2005GL025502, 2006.

De Angelis, S., and Bodin, P.: Watching the Wind: Seismic Data Contamination at Long Periods due to Atmospheric Pressure-Field-Induced Tilting, Bull. Seismol. Soc. Am., 102, https://doi.org/10.1785/0120110245, 2012.

Del Bello, E., Llewellin, E. W., Taddeucci, J., Scarlato, P., and Lane, S. J.: An analytical model for gas overpressure in slug-driven explosions: Insights into Strombolian volcanic eruptions, J. Geophys. Res.: Solid Earth, 117(B2), https://doi.org/10.1029/2011JB008747, 2012.

Diaz-Moreno, A., Iezzi, A. M., Lamb, O. D., Fee, D., Kim, K., Zuccarello, L., and De Angelis, S.: Volume Flow Rate Estimation for Small Explosions at Mt. Etna, Italy, From Acoustic Waveform Inversion, Geophys. Res. Lett., 46, https://doi.org/10.1029/2019GL084159, 2019.

Di Traglia, F., Berardino, P., Borselli, L., Calabria, P., Calvari, S., Casalbore, D., et al.: Generation of deposit-derived pyroclastic density currents by repeated crater rim failures at Stromboli Volcano (Italy), Bull. Volcanol., 86, https://doi.org/10.1007/s00445-024-01516-0, 2024.

Delle Donne, D., Tamburello, G., Aiuppa, A., Bitetto, M., Lacanna, G., D'Aleo, R., and Ripepe, M.: Exploring the explosive-effusive transition using permanent ultraviolet cameras, J. Geophys. Res.: Solid Earth, 122(6), 4377–4394, https://doi.org/10.1002/2017JB014027, 2017.

European Centre for Medium-Range Weather Forecasts (ECMWF), ECMWF Reanalysis v5. Available at: https://www.ecmwf.int/en/forecasts/dataset/ecmwf-reanalysis-v5. Access date: 21 July 2024.

Fee, D., Izbekov, P., Kim, K., Yokoo, A., Lopez, T., Prata, F., Kazahaya, R., Nakamichi, H., and Iguchi, M.: Eruption mass estimation using infrasound waveform inversion and ash and gas measurements: Evaluation at Sakurajima Volcano, Japan, Earth Planet. Sci. Lett., 480, https://doi.org/10.1016/j.epsl.2017.09.043, 2017.

Fee, D., Toney, L., Kim, K., Sanderson, R. W., Iezzi, A. M., Matoza, R. S., De Angelis, S., Jolly, A. D., Lyons, J. J., and Haney, M. M.: Local Explosion Detection and Infrasound Localization by Reverse Time Migration Using 3-D Finite-Difference Wave Propagation, Front. Earth Sci., 9, https://doi.org/10.3389/feart.2021.640202, 2021.

Francalanci, L., Tommasini, S., and Conticelli, S.: The volcanic activity of Stromboli in the 1906–1998 AD period: mineralogical, geochemical and isotope data relevant to the understanding of the plumbing system, J. Volcanol. Geotherm. Res., 131, https://doi.org/10.1016/S0377-0273(03)00364-1, 2004.

Francalanci, L., Davies, G. R., Lustenhouwer, W., Tommasini, S., Mason, P. R. D., and Conticelli, S.: Intra-Grain Sr Isotope Evidence for Crystal Recycling and Multiple Magma Reservoirs in the Recent Activity of Stromboli Volcano, Southern Italy, J. Petrol., 46, https://doi.org/10.1093/petrology/egi062, 2005.

Genco, R., and Ripepe, M.: Inflation-deflation cycles revealed by tilt and seismic records at Stromboli volcano, Geophys. Res. Lett., 37, https://doi.org/10.1029/2009GL042925, 2010.

Giordano, G., and De Astis, G.: The summer 2019 basaltic Vulcanian eruptions (paroxysms) of Stromboli, Bull. Volcanol., 83, https://doi.org/10.1007/s00445-020-01403-0, 2020.

Giudicepietro, F., Calvari, S., De Cesare, W., Di Lieto, B., Di Traglia, F., Esposito, A. M., Orazi, M., Romano, P., Tramelli, A., Nolesini, T., Casagli, N., Calabria, P., and Macedonio, G.: Seismic and thermal precursors of crater collapses and overflows at Stromboli volcano, Sci. Rep., 13, https://doi.org/doi.org/10.1038/s41598-023-38205-7, 2023.

Giudicepietro, F., López, C., Macedonio, G., Alparone, S., Bianco, F., Calvari, S., ... and Tramelli, A.: Geophysical precursors of the July-August 2019 paroxysmal eruptive phase and their implications for Stromboli volcano (Italy) monitoring, Sci. Rep., 10, 10296, https://doi.org/10.1038/s41598-020-67220-1, 2020.

Gheri, D., Zuccarello, L., De Angelis, S., Ricci, T., and Civico, R.: Infrasonic Data from the July 4–11, 2024 Paroxysm of Stromboli Volcano [Data set]. Zenodo. https://doi.org/10.5281/zenodo.14245572, 2024.

Gurioli, L., Harris, A. J. L., Colò, L., Bernard, J., Favalli, M., Ripepe, M., and Andronico, D.: Classification, landing distribution, and associated flight parameters for a bomb field emplaced during a single major explosion at Stromboli, Italy, Geology, 41, https://doi.org/10.1130/G33576.1, 2013.

Harris, A., and Ripepe, M.: Temperature and dynamics of degassing at Stromboli, J. Geophys. Res.: Solid Earth, 112(B3), https://doi.org/10.1029/2006JB004393, 2007.

INGV Bulletin of 25/06/2024: https://www.ct.ingv.it/index.php/monitoraggio-e-sorveglianza/prodotti-del-monitoraggio/bollettini-settimanali-multidisciplinari/914-bollettino-Settimanale-sul-monitoraggio-vulcanico-geochimico-e-sismico-del-vulcano-Stromboli-del-2024-06-25/file, last access: 19 August 2024.

INGV Bulletin of 02/07/2024: https://www.ct.ingv.it/index.php/monitoraggio-e-sorveglianza/prodotti-del-monitoraggio/bollettini-settimanali-multidisciplinari/915-bollettino-Settimanale-sul-monitoraggio-vulcanico-geochimico-e-sismico-del-vulcano-Stromboli-del-2024-07-02/file, last access: 19 August 2024.

INGV Bulletin of 09/07/2024: https://www.ct.ingv.it/index.php/monitoraggio-e-sorveglianza/prodotti-del-monitoraggio/bollettini-settimanali-multidisciplinari/918-bollettino-Settimanale-sul-monitoraggio-vulcanico-geochimico-e-sismico-del-vulcano-Stromboli-del-2024-07-09/file, last access: 19 August 2024.

INGV Bulletin of 16/07/2024: https://www.ct.ingv.it/index.php/monitoraggio-e-sorveglianza/prodotti-del-monitoraggio/bollettini-settimanali-multidisciplinari/920-bollettino-Settimanale-sul-monitoraggio-vulcanico-geochimico-e-sismico-del-vulcano-Stromboli-del-2024-07-16/file, last access: 19 August 2024.

James, M. R., Lane, S. J., and Chouet, B. A.: Gas slug ascent through changes in conduit diameter: Laboratory insights into a volcano-seismic source process in low-viscosity magmas, J. Geophys. Res.: Solid Earth, 111, https://doi.org/10.1029/2005JB003718, 2006.

Kim, K., and Lees, J. M.: Local Volcano Infrasound and Source Localization Investigated by 3D Simulation, Seismol. Res. Lett., 85, https://doi.org/10.1785/0220130135, 2014.

Legrand, D., and Perton, M.: What are VLP signals at Stromboli volcano? J. Volcanol. Geotherm. Res., 421, https://doi.org/10.1016/j.jvolgeores.2021.107429, 2022.

Longo, R., Lacanna, G., Innocenti, L., and Ripepe, M.: Artificial Intelligence and Machine Learning Tools for Improving Early Warning Systems of Volcanic Eruptions: The Case of Stromboli, IEEE Trans. Pattern Anal. Mach. Intell., 46(12), 7973–7982, https://doi.org/10.1109/TPAMI.2024.3399689, 2024.

Marchetti, E., and Ripepe, M.: Stability of the seismic source during effusive and explosive activity at Stromboli Volcano, Geophys. Res. Lett., 32, https://doi.org/10.1029/2005GL023962, 2005.

Marchetti, E., Genco, R., and Ripepe, M.: Ground deformation and seismicity related to the propagation and drainage of the dyke feeding system during the 2007 effusive eruption at Stromboli volcano (Italy), J. Volcanol. Geotherm. Res., 182, https://doi.org/10.1016/j.jvolgeores.2009.01.029, 2009.

McKee, K. F., Roman, D. C., Waite, G. P., and Fee, D.: Silent very long period seismic events (VLPs) at Stromboli Volcano, Italy, Geophys. Res. Lett., 49(23), e2022GL100735, https://doi.org/10.1029/2022GL100735, 2022.

McNutt, S. R., and Nishimura, T.: Volcanic tremor during eruptions: Temporal characteristics, scaling and constraints on conduit size and processes, J. Volcanol. Geotherm. Res., 178, https://doi.org/10.1016/j.jvolgeores.2008.07.023, 2008.

Pino, N. A., Moretti, R., Allard, P., and Boschi, E.: Seismic precursors of a basaltic paroxysmal explosion track deep gas accumulation and slug upraise, J. Geophys. Res.: Solid Earth, 116, https://doi.org/10.1029/2011JB008547, 2011.

Pistolesi, M., Delle Donne, D., Pioli, L., Rosi, M., and Ripepe, M.: The 15 March 2007 explosive crisis at Stromboli volcano, Italy: Assessing physical parameters through a multidisciplinary approach, J. Geophys. Res., 116, https://doi.org/10.1029/2011JB008527, 2011.

Ripepe, M.: Evidence for gas influence on volcanic seismic signals recorded at Stromboli, J. Volcanol. Geotherm. Res., 70, https://doi.org/10.1016/0377-0273(96)00033-8, 1996a.

Ripepe, M., Poggi, P., Braun, T., and Gordeev, E.: Infrasonic waves and volcanic tremor at Stromboli, Geophys. Res. Lett., 23, https://doi.org/10.1029/96GL02394, 1996b.

Ripepe, M., and Gordeev, E.: Gas bubble dynamics model for shallow volcanic tremor at Stromboli, J. Geophys. Res.: Solid Earth, 104, https://doi.org/10.1029/1998JB900046, 1999.

Ripepe, M., Delle Donne, D., Lacanna, G., Marchetti, E., and Ulivieri, G.: The onset of the 2007 Stromboli effusive eruption recorded by an integrated geophysical network, J. Volcanol. Geotherm. Res., 182(3-4), 131–136, https://doi.org/10.1016/j.jvolgeores.2009.02.011, 2009.

Ripepe, M., Delle Donne, D., Genco, R., Maggio, G., Pistolesi, M., Marchetti, E., Lacanna, G., Ulivieri, G., and Poggi, P.: Volcano seismicity and ground deformation unveil the gravity-driven magma discharge dynamics of a volcanic eruption, Nat. Commun., 6(1), 6998, https://doi.org/10.1038/ncomms7998, 2015.

Ripepe, M., Pistolesi, M., Coppola, D., Delle Donne, D., Genco, R., Lacanna, G., ... and Valade, S.: Forecasting effusive dynamics and decompression rates by magmastatic model at open-vent volcanoes, Sci. Rep., 7, https://doi.org/10.1038/s41598-017-00748-4, 2017.

Ripepe, M., Lacanna, G., Pistolesi, M., Silengo, M. C., Aiuppa, A., Laiolo, M., ... and Delle Donne, D.: Ground deformation reveals the scale-invariant conduit dynamics driving explosive basaltic eruptions, Nat. Commun., 12, 1683, https://doi.org/10.1038/s41467-021-21722-2, 2021a.

Ripepe, M., Delle Donne, D., Legrand, D., Valade, S., and Lacanna, G.: Magma pressure discharge induces very long period seismicity, Sci. Rep., 11, https://doi.org/10.1038/s41598-021-86061-x, 2021b.

Ripepe, M., and Lacanna, G.: Volcano generated tsunami recorded in the near source, Nat. Commun., 15, https://doi.org/10.1038/s41467-024-18567-x, 2024.

Rizzo, A. L., Federico, C., Inguaggiato, S., Sollami, A., Tantillo, M., Vita, F., ... and Grassa, F.: The 2014 effusive eruption at Stromboli volcano (Italy): Inferences from soil CO_2 flux and $^{3}He/^{4}He$ ratio in thermal waters, Geophys. Res. Lett., 42, https://doi.org/10.1002/2015GL064152, 2015.

Rosi, M., Bertagnini, A., Harris, A. J. L., Pioli, L., Pistolesi, M., and Ripepe, M.: A case history of paroxysmal explosion at Stromboli: Timing and dynamics of the April 5, 2003 event, Earth Planet. Sci. Lett., 243, https://doi.org/10.1016/j.epsl.2006.01.035, 2006.

Rosi, M., Pistolesi, M., Bertagnini, A., Landi, P., Pompilio, M., and Di Roberto, A.: Chapter 14 Stromboli volcano, Aeolian Islands (Italy): present eruptive activity and hazards, Geol. Soc., London, Mem., 37, https://doi.org/10.1144/M37.14, 2013.

Sparks, R. S. J.: Dynamics of magma degassing, Geol. Soc., London, Spec. Publ., 213, https://doi.org/10.1144/GSL.SP.2003.213.01.07, 2003.

Suckale, J., Keller, T., Cashman, K. V., and Persson, P.-O.: Flow-to-fracture transition in a volcanic mush plug may govern normal eruptions at Stromboli, Geophys. Res. Lett., 43, https://doi.org/10.1002/2016GL068082, 2016.

Wang, S.: Finite-difference time-domain approach to underwater acoustic scattering problems, J. Acoust. Soc. Am., 99, https://doi.org/10.1121/1.414620, 1996.